Battery Cell-to-Pack Scaling Trends for Electric Aircraft

Jeffrey C. Chin*, Karsten Look†, Ezra O. McNichols †
Dustin L. Hall*, Justin S. Gray*, Sydney L. Schnulo*
NASA Glenn Research Center, Cleveland, OH, 44135

Battery pack gravimetric energy density is one of the most important, yet often miss-estimated, design parameters for sizing all-electric aircraft. Proper accounting for thermal, structural, and operational safety margins are frequently lost when extrapolating performance from the cell level to the aircraft level. This paper summarizes the relevant engineering and certification details needed to better account for the penalties associated with assembling battery packs. The overhead penalty when scaling from cell to pack energy density is not constant, as is often assumed. Furthermore, the scaling relationship varies depending on pack requirements, cell chemistry, and architecture. Parametric, high-fidelity models are used to determine optimal battery pack sizes over a range of conditions to better quantify technology scaling effects. Simply stated, doubling cell energy density doesn't translate to doubled pack energy density.

I. Nomenclature

A	=	amperes (A)
$^\circ C$	=	degrees Celsius ($^\circ C$)
CD	=	rapid discharge capacity
$C-rate$	=	discharge C-rate (A)
CS	=	crash safety
D_{cell}	=	cylindrical cell diameter (mm)
ϵ	=	battery gravimetric energy density ($\frac{W*hr}{kg}$)
η	=	efficiency
EC	=	explosion containment
HT	=	high temperature
κ	=	thermal conductivity ($\frac{W}{mK}$)
I	=	current (A)
P	=	power (kW)
R_{elec}	=	range (km)
R	=	internal cell resistance (ohm)
RD	=	rapid decompression
s	=	spacing, core padding width to cell diameter ratio
SOC	=	state-of-charge
t	=	time (s)
T	=	temperature (K)
TR	=	thermal runaway
TS	=	temperature shock
v	=	test function
w	=	pack column/row width (mm)
Wh	=	watt hours ($W*hr$)

*Propulsion Systems Analysis Branch, AIAA Member
†Turbomachinery and Turboelectric Systems Branch

II. Introduction

Due to the long development cycles for aircraft, designers attempt to forecast future attainable battery densities based on roadmaps published for various cell chemistries. The lack of publicly released electric aircraft battery pack-level solutions gives vehicle designers minimal empirical data points to extrapolate results to future technologies. The X-57 battery is a common reference, using 225 Wh/kg lithium-ion cells to create a 149Wh/kg pack[1]. The terms pack, battery, and battery pack are used somewhat interchangeably here to refer to the entire energy storage system including packaging.

Two assumptions are typically made when predicting battery weight. First, for a given pack architecture, weight of the pack will scale linearly with required energy. This assumption is generally accurate within certain ranges. Small exceptions occur due to discrete changes in weights for the battery management system (BMS) or for venting, mounting, etc. At a high-level, if one needs to double the number of cells, the overhead also doubles; essentially, the pack could be created from two instances of the original battery pack size. The second common assumption is that the percentage knockdown from cell energy density to pack energy density remains constant as cells improve. This assumption can be much less accurate, as is visualized on the green dashed curve in Figure 1.

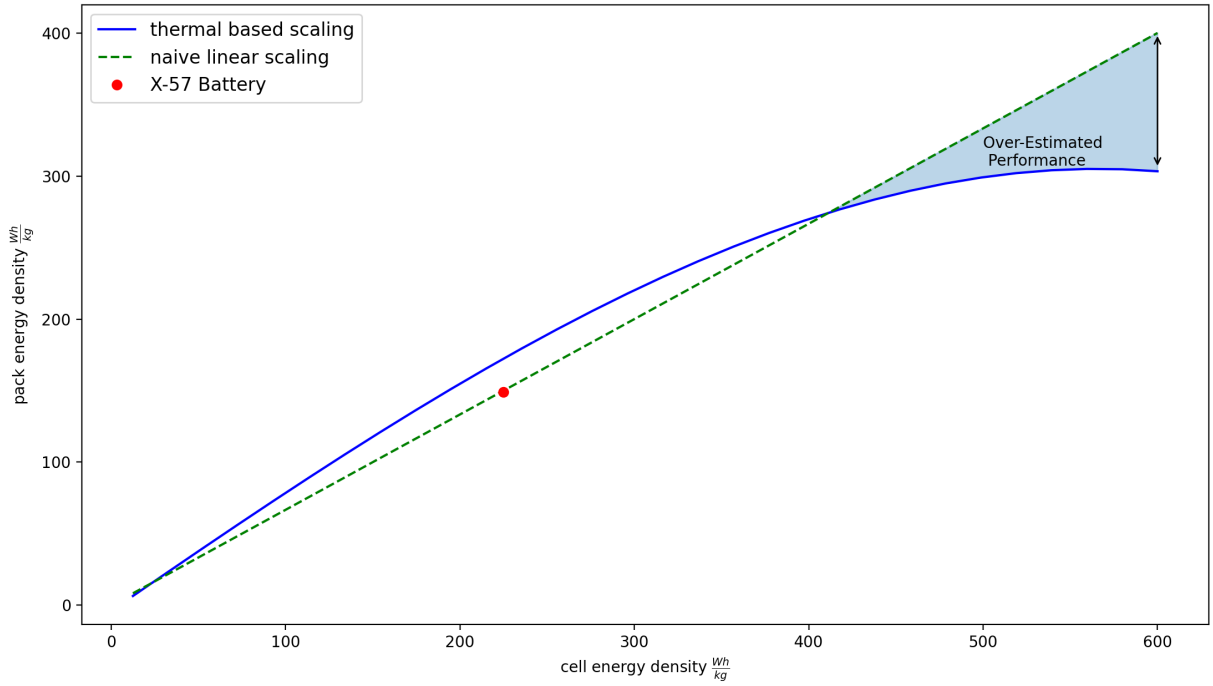

Fig. 1 Comparison of Scaling Assumptions

If a designer expects cell energy density to double in the next five years, they might assume the achievable pack energy density is also doubled. If total battery pack capacity remains fixed, the number of cells required would be halved and the overhead mass would also need to be halved to achieve doubled energy density. However, a substantial amount of the overhead exists to prevent thermal runaway, and the absolute energy contained within the pack has not changed. Cutting the overhead in half means the material would need to suddenly be twice as effective at diffusing thermal energy and containing thermal runaway. If packaging innovation and material property improvements advance as fast as cell chemistry improvements, following the green trendline is still possible. Otherwise pack energy density will likely trail in performance as cell technology improves, as shown by the blue curve in Figure 1. This thermal based scaling trendline is the result of numerous individual design optimizations across a range of cell energy densities, contained within an aluminum core.

Another common pitfall is focusing on managing nominal heat loads and neglecting thermal runaway completely. These solutions are often advertised as being lightweight with high thermal performance, but fail to include any considerations for runaway scenarios. Understanding the extent of nominal heat loads is important and covered in previous works [1]. Additionally, it can be important for setting realistic initial conditions for simulating runaway events.

The remainder of this paper details what factors would help contribute to more accurate battery pack-level weight scaling, with minimal discussion of the cell chemistry itself. The points outlined here have two main repercussions to consider. First, energy storage innovation requires technology improvements beyond the cell itself; otherwise, improvements in cells can quickly be lost at the pack level. Second, pack level innovation is driven by trades at the vehicle level. These designs are multidisciplinary in nature, and the optimal battery pack architecture and size is often driven by multiple considerations beyond the cells.

III. Battery Standards Relevant to Weight Scaling Estimates

Battery pack design for aviation must conform to multiple standards which specify design approach, performance, environmental tolerance, and safety expectations. These standards often also include testing methods, pass/fail criteria, and key metrics that battery manufacturers must report.

These requirements have varying impacts on overall pack weight. Therefore, a review of the highest-impact items is necessary to sustain a full understanding of pack scaling performance. Table 1 lists the most directly relevant standards documents. Additional documents considered can be found in Appendix B.

Table 1 Documents Governing Lithium Battery Design in Aircraft

Designator	Title
AC 20-184	Guidance on Testing and Installation of Rechargeable Lithium Battery and Battery Systems on Aircraft [2]
JSC 20793 D	Crewed Space Vehicle Battery Safety Requirements [3]
RTCA DO-160G	Environmental Conditions and Test Procedures for Airborne Equipment [4]
RTCA DO-311A	Minimum Operational Performance Standards for Rechargeable Lithium Batteries and Battery Systems [5]
RTCA DO-347	Certification Test Guidance for Small and Medium Sized Rechargeable Lithium Batteries and Battery Systems [6]
TSO-C179a	Permanently Installed Rechargeable Lithium Cells, Batteries, and Battery Systems [7]
UN/DOT 38.3 T4	Manual of Tests and Criteria, Section 38.3 Lithium Metal and Lithium Ion Batteries [8]

Many of these documents share similar requirements. Those focusing on the thermal design of the battery pack that are most likely to govern thermal management system (TMS) weight are listed in Table 2. Table 3 indicates the shared requirements within the corpus. Military safety testing can be categorized into twelve individual tests, with seven being applicable to commercial applications. Of those tests, only a subset have significant influence on the battery pack weight.

Table 2 Key Requirements that Impact Weight*

Designator	Requirement	General Weight of Solution
CS	Crash Safety	high
TR	Prevention of Thermal Runaway	high
HT	High Temperature Test	med
CD	Rapid Discharge Capacity	med
EC	Explosion Containment	high
TS	Temperature Shock	low
RD	Rapid Decompression	med

Descriptions of key requirements

*1. Crash Safety **(CS)***

The crash safety test ensures the battery system does not create hazardous conditions for passengers during a hard landing or crash landing. This will impact weight requirements by increasing the amount of material needed to

Table 3 Requirements Distribution in Regulations Documents

Document	Requirement						
	CS	TR	HT	CD	EC	TS	RD
AC 20-184	x[2]	x[1]	x[1]	x[1]	x[1]	x[1]	x[2]
JSC 20793 D	*x*[3]	x	x	x	x		
RTCA DO-160G	x		x		x	x	x
RTCA DO-311A	x[2]	x	x	x	x	x	x[2]
RTCA DO-347	x[2]	x	x[2]	x		x[2]	
TSO-C179a	x[2]	x[1]	x[1]	x[1]	x[1]	x[1]	x[2]
UN/DOT 38.3 T4	x		x	x		x	

[1] References DO-311A
[2] References DO-160G
[3] References Launch Accelerations

structurally reinforce the walls and mounting points of the pack. Crash forces can be as large as a 20g acceleration over 11 ms.

*2. Prevention of Thermal Runaway **(TR)***

This requirement dictates the battery pack prevent self-sustaining, uncontrolled increases in temperature and pressure due to cell failure. In order to prevent cell failures from propagating due to thermal contact, the battery TMS must be sized to handle large heat transients. The weight of this system will scale with the total energy released during an individual cell failure.

*3. High Temperature Test **(HT)***

This test includes measuring pack capacity and performance when operating at an ambient temperature as high as 50°C. This puts significant thermal demands on the TMS. In general, as the temperature gradient decreases, the rate of heat transfer decreases. To maintain a minimum heat transfer effectiveness, the TMS must increase in size and weight.

*4. Rapid Discharge Capacity **(CD)***

This category of requirements specify the battery capacity at high discharge rates, up to 10C (the rate required to discharge the full battery in 1/10th of an hour, 6 minutes). This intensive loading will likely produce significant thermal loads from the pack due to resistive heating. The TMS must be sized to safely dissipate this heat during operation. The amount of heat to be removed correlates with the total energy capacity of the pack. *This is distinct from an "external short circuit" test in that current must flow uninterrupted from the battery.* In a short circuit test, current may be interrupted by a circuit breaker or similar interrupting or current-limiting device.

*5. Explosion Containment **(EC)***

The explosion containment test requires that, in the event of a single-cell Thermal Runaway (TR) event, all solid debris and flame is contained within the battery casing. Venting of gas and liquids is permitted in DO-311A. Weight considerations ensure the structural integrity of the walls is sufficient to withstand the increased pressure due to the generation of gasses during a TR.

*6. Temperature Shock **(TS)***

This test verifies the effectiveness of the battery components when exposed to extreme temperature fluctuations, such as those encountered in flight. Temperature swings can range from -55°C to 80°C within a very short interval. Weight considerations would include adequate sizing of the structure to withstand thermal stresses and maintain seals.

*7. Rapid Decompression **(RD)***

This test evaluates the ability of seals and vents to compensate for a step-wise rapid pressure change in the event of a battery undergoing rapid decompression from within the pressurized volume of the aircraft. This requirement imposes a weight penalty to ensure the battery casing will not rupture during the pressure change. Larger batteries with increased interior surface areas will require greater structural support.

IV. Pack Modeling Approach

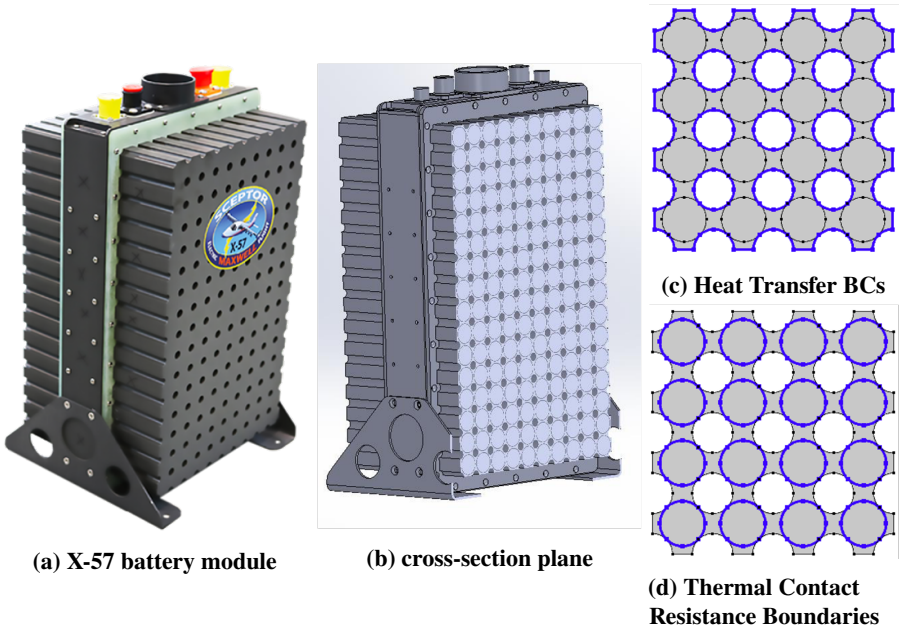

(a) X-57 battery module **(b) cross-section plane** **(c) Heat Transfer BCs** **(d) Thermal Contact Resistance Boundaries**

Fig. 2 Solid Core Battery Pack Architecture Represented as an Extruded 2D Cross-Section

The remainder of the paper will focus on the weight impact of thermal runaway prevention. All three requirements identified above as having high weight impact (CS, TR, EC) have considerations that are quite implementation dependent. However, the most basic ways in which thermal runaway can be avoided are relatively straightforward to model in a generalized way. A common aviation battery architecture encapsulates cells around a solid body of material. This interstitial solid core both prevents multi-cell propagation events and provides substantial mass to distribute the resulting high thermal load from a single-cell event. The Maxwell X-57 vehicle and Embry Riddle HK36 vehicle both use solid core packs, the former made from aluminum and the latter from a phase change composite.[9] The Orion and LLB-2 battery modules are also constructed similarly, with the cells staggered diagonally, akin to honeycomb, rather than arranged in a square grid [10]. Both configurations are examined here.

To fully understand how pack structure scales with energy density, high-fidelity thermal and structural simulations are used to determine the lightest pack geometry for various energy densities and design scenarios. Figure 2 shows a simplified 2D cross-section of the X-57 battery, which is further reduced to a small tessellated region of effect to rapidly evaluate various designs. This parametric geometry is used to perform size optimization, with geometry parameters defined in Figure 3 for both the grid layout variant and the staggered honeycomb or hexagonal layout.

In both of these layouts, the geometry and thermal transient can be defined based on the parameters of interest listed in Table 4. The optimization is performed using two geometry design variables: 1) the spacing between the cells and 2) the size of the internal cutouts, denoted as "holes". Rather than modeling the entire pack, it is assumed that a smaller subset of cells will exhibit the same behavior in an area around the location of a thermal runaway. Adding more cells wouldn't significantly change the outcome, but would increase the simulation time required. Determining the minimum number of cells necessary to model is dependent on the total thermal resistance between each of the neighboring cells.

Figure 3 also shows the location of the cell assumed to enter thermal runaway. The corner cell is used for both geometries considering it is the worst case scenario if no cooling is applied to any surface. In a simplified adiabatic model, the pack can only rely on diffusing energy through the remainder of the pack, and the corner cell has the least

mass surrounding it. Further studies could consider variable amounts of surface cooling, which would also impact the starting temperature distribution within the pack. These hypothetical situations are only briefly considered here, since the overall non-linear pack density scaling trends can be demonstrated without enumerating all of these scenarios.

To ensure a more numerically stable optimization, careful consideration is required for defining the geometry. Rather than choosing all dimensions independently, each parameter is normalized to the diameter of the cell. This ensures the optimizer cannot inadvertently select an infeasible geometry. As an example, the hole ratio variable can be any real number between zero and one, with one being the maximum available hole size. This makes the hole features dependent on both the spacing and ratio variable with the absolute diameter calculated as $D_{hole} = ratio * D_{cell} * (\sqrt{2} * s - 1)$ where $s = \frac{w}{D_{cell}}$ for the grid design.

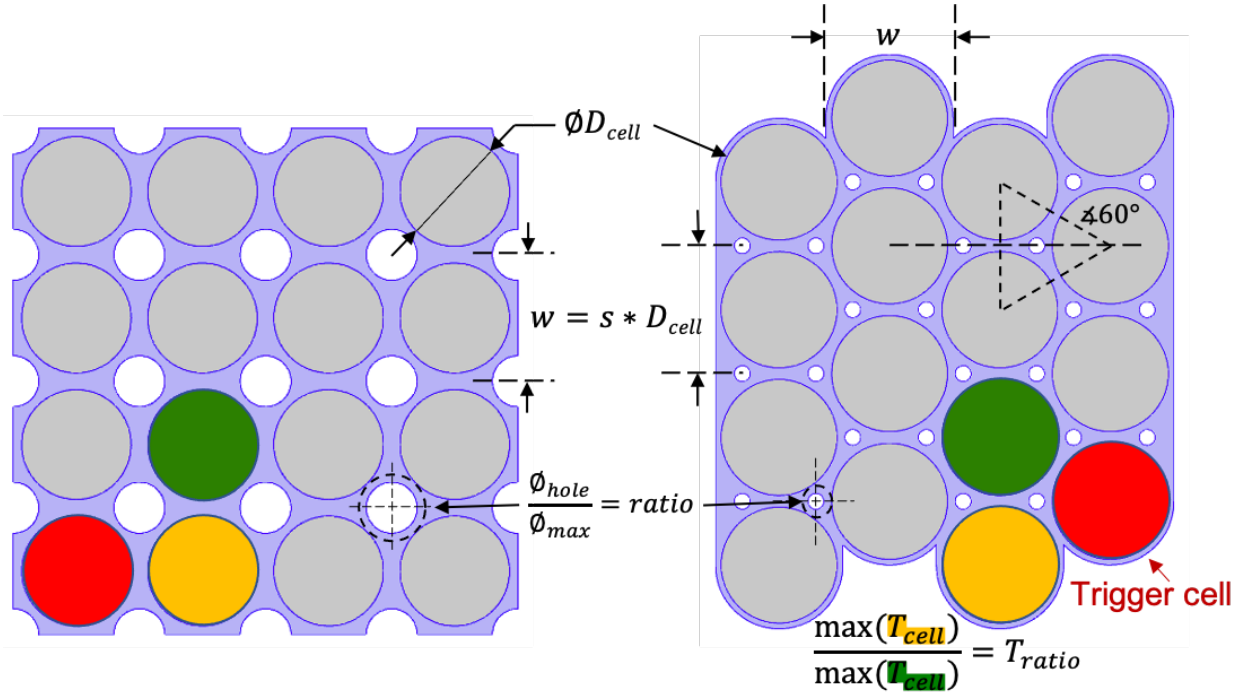

Fig. 3 Grid vs. Honeycomb Dimensions and Temperature Locations. Core Shown in Purple; Cells in Gray

In the honeycomb arrangement, the cells are staggered, with columns horizontally offset by a distance of $\frac{w*\sqrt{3}}{2}$ and vertically offset by a distance of $\frac{w}{2}$ to form equilateral triangles between cell midpoints.

Simply adjusting two of these parameters can lead to drastically different designs as show in Figure 4.

Table 4 Battery Pack Design Parameters

Parameter	Description	Value/Range/Units
D_{cell}	cell diameter	18 (mm)
s	spacing between cells, normalized by cell diameter	$\mathbb{R}_{\geq 1}$ (unitless)
ratio	ratio of hole diameter to available space	$\{x \in \mathbb{R} \mid 0 \leq x \leq 1\}$ (unitless)
n_{cells}	number of cells in the vertical grid direction	$\mathbb{Z}^+$ (unitless)
m_{cells}	number of cells in the horizontal grid direction	$\mathbb{Z}^+$ (unitless)
$R_{contact}$	thermal contact resistance	$(1-5) * 10^{-3}$ $(\frac{K*m^2}{W})$
$load_{heat}$	thermal energy released into the case during runaway	10-30 (kJ)
k_{body}	thermal conductivity of the solid core	10-201 $(\frac{W}{m*K})$
k_{cell}	thermal conductivity of the battery cell	96 $(\frac{W}{m*K})$

By giving an optimizer control of the geometry, a mass optimal shape can be determined for any given cell size, material property, thermal condition and/or limit imposed. The optimization problem formulation for the baseline results are to minimize overall pack mass, with respect to sizing and ratio design variables, subject to a peak neighboring cell temperature of 340K, and a maximum peak temperature ratio of 1.1 between adjacent cells, designated in Figure 3. The computational flow and data passing are visually charted using the eXtended Design Structure Matrix (XDSM) notation [11] in Figure 5.

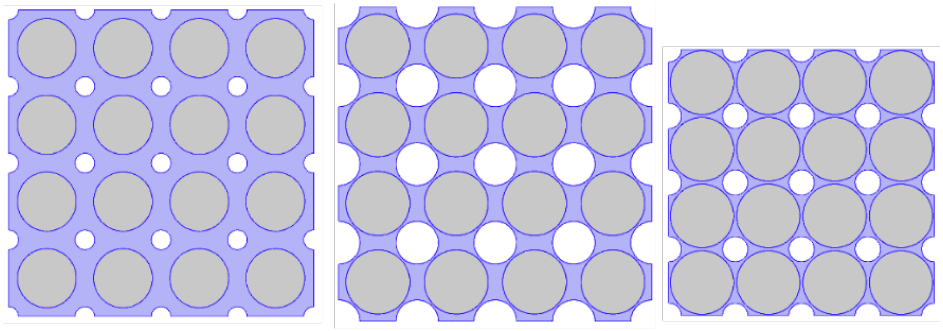

Fig. 4 Examples of variations using only two geometry variables (hole ratio and spacing), without changing cell size

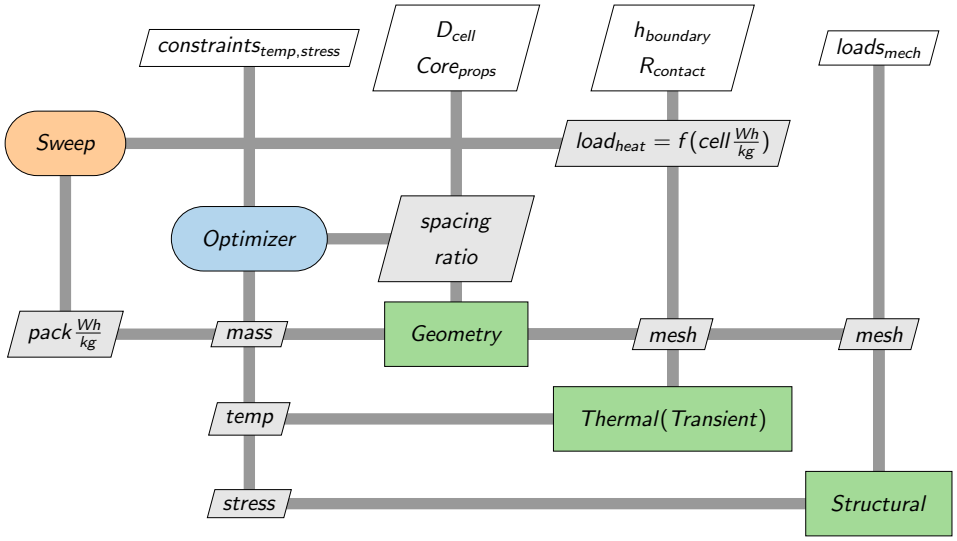

Fig. 5 Design structure (XDSM) for determining the optimal pack design for a sweep of inputs.

The optimal shape is highly dependent on the imposed constraints. Simply imposing a maximum neighboring cell temperature results in a design with very large spacing between cells with long and narrow thermal paths between them. This type of design would effectively isolate cells, but drastically hurts the volumetric energy density of the pack. It would also diminish the total effective thermal capacity of the pack since uneven heat loads would have difficulty spreading through the entire core mass.

Adding insulation between the cell body and the pack core would similarly achieve lower neighboring cell temperatures during runaway, but would trap heat within the cells under normal operation. Therefore, packs can't be sized exclusively for thermal runaway, but also must meet constraints for nominal thermal and structural performance. This creates conflicting interest when sizing cell containment material. On one hand, the designer wants to encourage heat spread from the cell to the body, reducing thermal isolation of the cells. On the other hand, the cells must be isolated as much as possible during thermal runaway. These competing interests combined with structural and volume constraints make the design process ideal for multidisciplinary design optimization and analysis (MDAO) tool-sets.

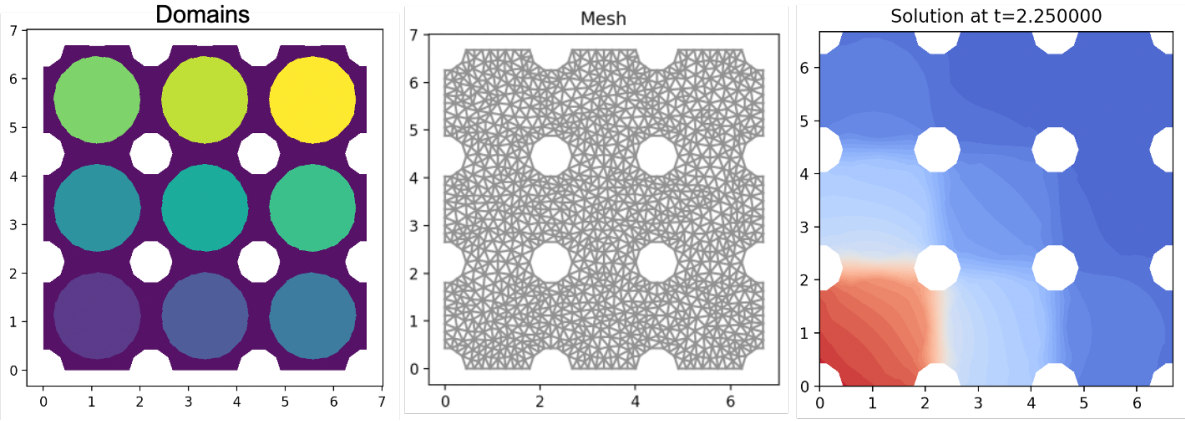

Fig. 6 Automatic resizing, to mesh generation, to FEM simulation

Picking a constraint to meet nominal thermal performance can be challenging because the definition of normal operation varies greatly between applications and missions. Thermal runaway constraints are easier to quantify, as they are often better defined and related directly to material properties.

To quantify the spread of the core heat in simple terms, the percent difference in max temperature between a vertically adjacent cell and diagonally adjacent cell are compared. The cells of interest are marked yellow and green in Figure 3. By limiting the temperature gradient between neighboring cells during runaway, the optimizer is forced to rely more heavily on thermal capacity to reduce peak temperature rather than thermal isolation.

High fidelity modeling is performed with two separate tools to ensure computational agreement and broaden model accessibility. The PDE has been implemented in both COMSOL multi-physics software as well as the open-source FENICS platform [12]. The problem is set up identically in each environment, solving the following underlying transient heat equation PDE.

$$\int_{\Omega} \frac{u^{k+1} - u^{k}}{k} v \, dx = -\int_{\Omega} \kappa \nabla \mathrm{um} \cdot \nabla v \, dx.$$

where $u = u(x,t)$ is the thermal capacity at location $x \in \Omega$ and time $t \in [0,T]$, with a test function v. The $\theta-$method for the time discretization is used with $u \approx \mathrm{um} := \theta\, u^{k+1} + (1-\theta)\, u^{k}$ with $\theta \in [0,1]$. κ is the thermal conductivity.

V. Thermal Modeling Assumptions

The amount of energy released by a cell during thermal runaway has been extensively researched for cylindrical format cells, although it has been found to be a highly stochastic phenomena. [13] Generally speaking, as the energy density or capacity of the cell increases, the runaway energy released from the cell also increases. Data taken from fractional calorimetry experiments shows that 20kJ of heat released per Amp-hour of capacity is a good first estimate for high energy cells. [13] However, there is much more variation in the percentage of that energy that is transmitted to the surrounding pack material versus ejected as hot gas. Anywhere between 20 and 70 percent of the energy is ejected as gas, with higher ejection rates being defined as having proportionally less energy thermally disbursed within the pack. Techniques for reliably reducing the transmitted heat to the cell case would certainly benefit system performance, making it an ideal candidate for future study. In this study, all of these factors are reduced down to using the energy density of the cell (in $\frac{Wh}{kg}$) divided by a factor 12.5 to approximate the heat load (in kJ) absorbed by the pack.

Solutions are also sensitive to the thermal properties of the cell, which can be challenging to measure across many chemistry types and manufacturers. For this analysis, cell properties are characterized as separate bulk anisotropic properties based on materials, which differ in the radial and axial directions. [14] The bulk thermal capacity is conservatively assumed to be 0.8 $\frac{J}{gK}$ [15], and the axial thermal conductivity is assumed to be 28 $\frac{W}{mk}$. [16] The radial thermal conductivity through the layers of the wound anode and cathode laminations varies widely in literature from 0.4 to 3.0 $\frac{W}{mk}$. [17] The temperature threshold where self-heating and propagation begins is chosen to be 135 °C. Thermal resistance between the active layers, case, liner, and core is lumped into a single value, with an assumed 0.05mm of

Kapton adding 1.9 $\frac{C}{W}$ and 0.75 $\frac{C}{W}$ kapton-to-metal resistance. [18]

Structural modeling considerations were also briefly considered but were found to never be an active constraint for a square cell arrangement. Even a highly conservative 20g acceleration load simultaneously applied both downward and laterally did not violate a constraint on maximum Von-Mises stress within the core structure. For many aeronautic applications, such as X-57, loads do not exceed 5g in any direction. Since these geometries ignore fastener design, the model overlooks potential stress points coming from mounting locations. Artificially high stresses can be a symptom of finite element mesh resolution around sharp corners, so results around the boundaries are ignored when appropriate. Although mounting designs are beyond the scope of this paper, the same analysis workflow could be applied with more detailed designs.

VI. Results

Many of these trends are dependent on the specific combination of model inputs used. As such, it is not feasible to present the entire design space. Key trends are discussed, but the absolute values for pack densities should not be interpreted as theoretical maximum limits.

A. Baseline Energy Density Scaling

Contour plots showing how the two shape design variables impact the constraints and objective are shown below. The regions where all the contours overlap signify the feasible region, with the mass objective being minimized closest to the bottom right of the graph. As the energy density increases, the temperature contour region shrinks the feasible space shown in Figure 7.

The cell spacing variable shown on the y-axis of each plot has a much greater impact on the temperature than the hole size ratio on the x-axis. It is possible for the neighboring cell temperature to be reduced without increasing mass by simultaneously increasing the spacing between cells and making the holes larger. Although this doesn't impact the energy density, it's undesirable from a volumetric energy density perspective. The design space can be further narrowed by activating a constraint on the total area of the pack or by including both side length and mass as parts of the objective function to be minimized.

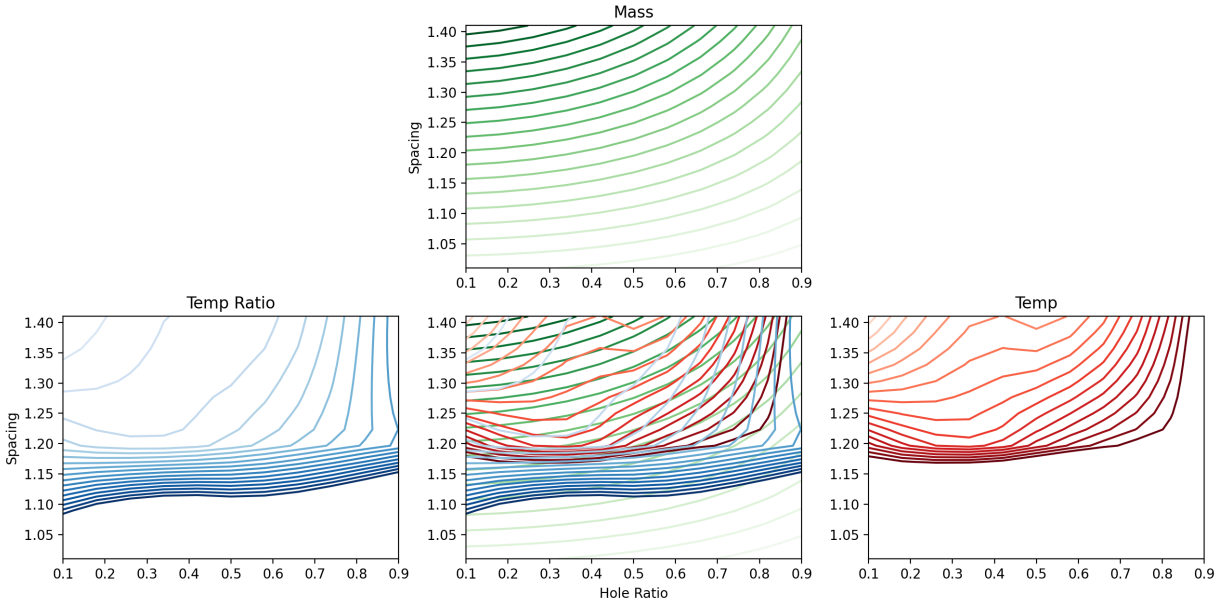

Fig. 7 Three Performance Metric Contours for the Spacing (y-axis) and Hole Ratio (x-axis) Design Variables, Overlaid in the Center. Lighter lines indicated improvement for each metric.

The optimization can then be ran over a sweep of cell energy densities, with the minimum mass pack computed at each point. Calculating the mass of each optimized point then allows the relationship between cell and pack energy

density to be determined as shown in Figure 8. The percentage of the pack dedicated to overhead materials is also plotted, showing that as energy density improves, a larger percentage of the pack must be dedicated to thermal management. As the energy density of the cells goes up, the amount of heat needing to be dissipated rises. A 200 and 400 $\frac{Wh}{kg}$ cell energy density corresponds to a 16 and 32 kJ core heat load, respectively.

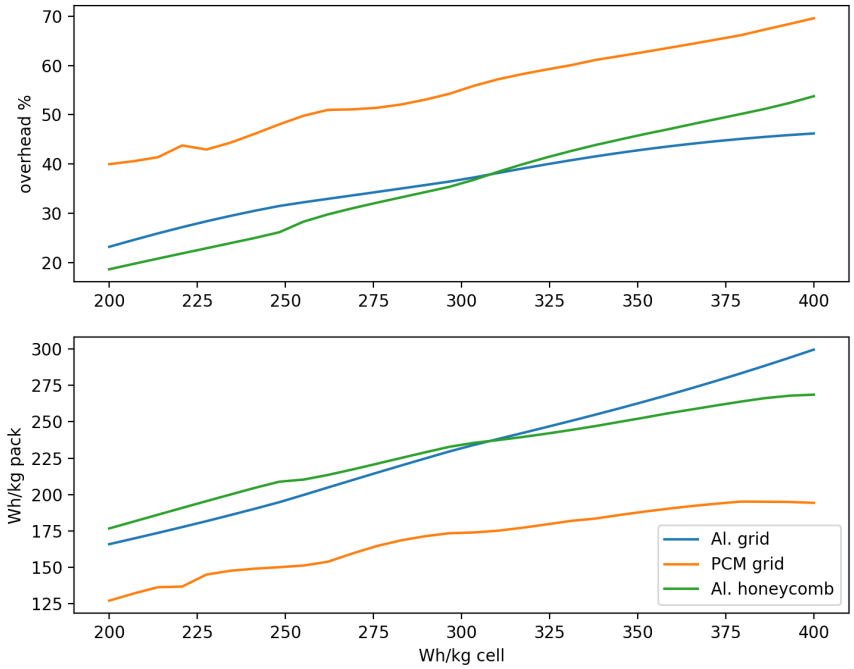

Fig. 8 Cell-to-pack scaling trends as energy density increases with multiple configurations shown.

B. Core Material Design Study

The second study performs the same analysis but with a different interstitial material between the cells. This time, a composite of phase change materials and graphite is used. This material is characterized by a appreciably higher latent heat than aluminum at the cost of a lower thermal conductivity. Core conductivity was reduced from 201 to 10 $\frac{W}{mK}$, and heat capacity was increased from 900 to 2000 $\frac{J}{kgK}$.

The optimal versions of this pack variant were heavier than the aluminum counterparts for every energy density as shown in Figure 8. This is attributed to the fact that, although the core can absorb more heat, much less of the material participates in the absorption since the heat remains localized.

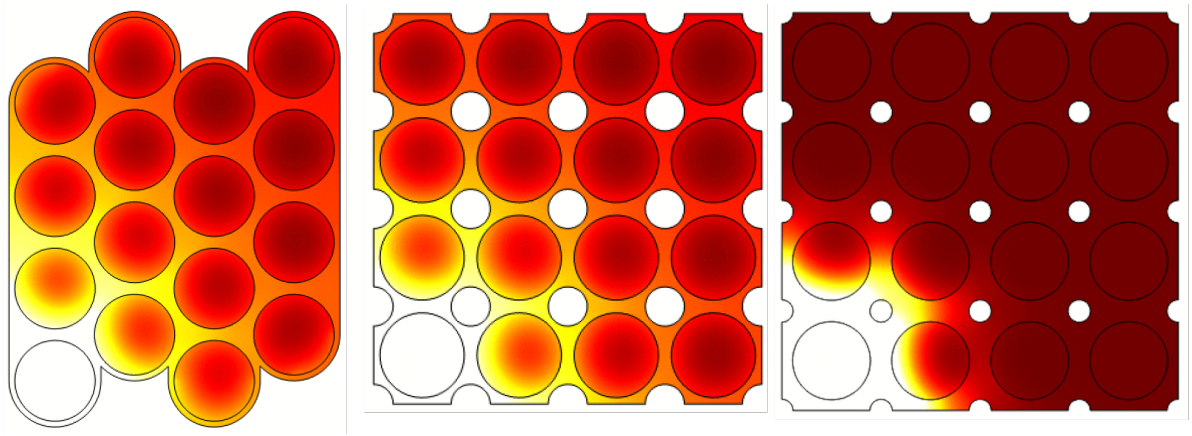

Fig. 9 Visualization of heat diffusion for various geometries and core materials. Color maps are held constant between images to show varying regions of effect. Left and center showing aluminum designs, right showing a phase change composite.

C. Geometry Design Study

The third study follows the same steps, for the staggered honeycomb geometry. At low energy densities, the honeycomb arrangement is more mass efficient. This is likely due to a less tortured path for transferring heat to the rest of the pack. Interestingly, there is a intersection point where the rectangular cell grid layout outperforms the honeycomb. At higher energy densities, the cells simply need to be further spaced out, and the grid geometry is able to achieve this without mass dramatically rising. In this comparison, the external heat transfer outside the core is assumed to be $10\frac{W}{m^2K}$ so the addition of holes does little to impact the outcome of the honeycomb design.

D. Surface Cooling Design Study

The fourth study only considers the staggered honeycomb design with holes, sweeping the boundary heat transfer coefficient between $10\frac{W}{m^2K}$ and $250\frac{W}{m^2K}$. The lowest coefficient represents natural convection, and the largest value represents high airflow or liquid cooling.

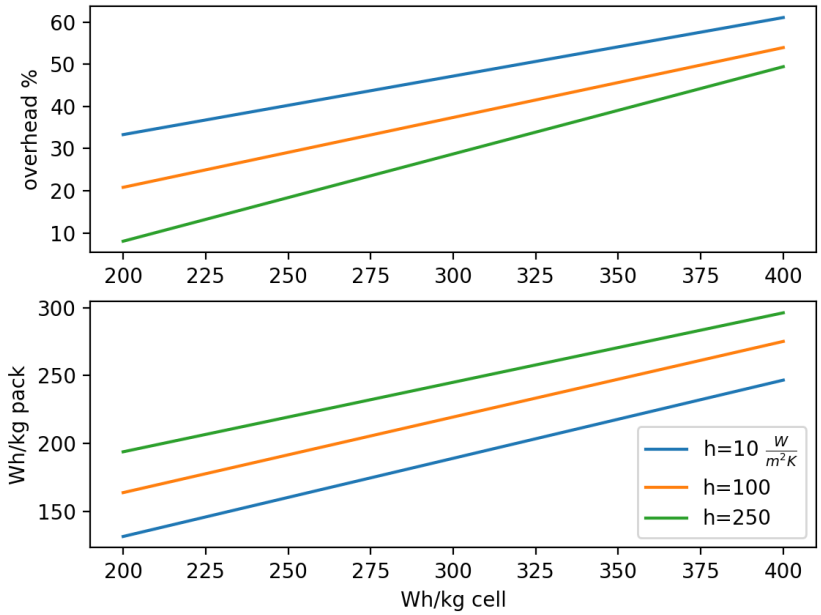

Fig. 10 Scaling trends for a honeycomb configuration with three levels of boundary cooling.

Linear trendlines in Figure 10 show that the optimal pack energy density sees a fairly consistent improvement with increased cooling across the range of cell energy densities. This particular trade does not consider any sort of increased weight penalty to achieve the higher cooling levels, so, in reality, the higher cooling trend would shift down. Assuming the weight impact of increased cooling isn't a function of cell energy density, this seems to indicate that active cooling would be less weight efficient on low energy density packs and not worth the added complexity.

These trends cannot be compared to the previous Figure 8 trends considering a lower temperature constraint of 330K was used to ensure an active constraint on the high cooling case at low cell energy densities. Although linear trendlines were appropriate within the smaller range shown above, these results also cannot be extrapolated beyond the ranges shown in the plots. If expanded, they would taper off in the same fashion as Figure 1.

VII. Conclusion

Increased battery cell energy density leads to more concentrated heat loads during thermal runaway. Pack overhead necessary to safely dissipate these loads similarly rises, causing pack energy density to fall behind improvements in cell energy density. A method to determine the optimal pack shape for a range of material options is presented. Although replacing aluminum core battery packs with phase change materials can improve the total energy absorption capacity, it can adversely impact pack overhead weight due to poor ability to effectively spread the heat throughout the pack. There is also no "golden-bullet" configuration that is optimal for all scenarios. The optimal choice of a grid versus a staggered cell packaging depends on the materials used, the cell energy density, and external cooling.

VIII. Future Work

Future work will examine new pack architectures using materials with advanced heat conduction and specific heat properties. As these properties are improved, a larger portion of the pack participates in spreading thermal loads, potentially requiring larger simulations. More sophisticated packs may also require more geometric variables making the design process even more tightly coupled.

To improve the numerical speed and stability of the optimization process, alternate high fidelity PDE solvers are also being considered. Modern university-developed software packages allow forward and backward derivative propagation, allowing the optimizer to make more efficient steps through the design space. As a first step, this requires analytic

derivatives when mapping geometric parameters to the mesh. Additionally, operations to map derivatives from the the mesh to functionals are needed. An example of this would be computing max temperature with respect to volume node position.

Additional application specific constraints and physics will also be explored, including structural batteries embedded within fuselage and wing structures in follow-on work. Volume specific considerations open up new variables for non-square packs, non-symmetric loads, and cooling boundaries. Taking all of these considerations into account beyond the cell design creates many opportunities for improved performance over current state-of-the-art pack design.

Acknowledgments

The authors would like to thank the NASA Transformational Technologies and Toolsets (TTT) for sponsoring this work and the X-57 team for providing the initial inspiration for this study.

References

[1] Chin, J. C., Schnulo, S. L., Miller, T. B., Prokopius, K., and Gray, J., "Battery Performance Modeling on Maxwell X-57," *AIAA Scitech 2019 Forum*, AIAA Aviation, American Institute of Aeronautics and Astronautics, 2019, p. 15. doi:doi:10.2514/6.2016-3920, URL https://arc.aiaa.org/doi/pdf/10.2514/6.2019-0784.

[2] *AC 20-184 - Guidance on Testing and Installation of Rechargeable Lithium Battery and Battery Systems on Aircraft*, Federal Aviation Administration, October 2015.

[3] "Crewed Space Vehicle Battery Safety Requirements," Tech. Rep. JSC-20793 D, NASA Johnson Space Center, Mar 2017.

[4] *Environmental Conditions and Test Procedures for Airborne Equipment*, Radio Technical Commission for Aeronautics (RTCA), Dec 2010. Document no. RTCA DO-160G.

[5] *Minimum Operational Performance Standards for Rechargeable Lithium Battery Systems*, Radio Technical Commission for Aeronautics (RTCA), Mar 2008. Document no. RTCA DO-311.

[6] *Certification Test Guidance for Small and Medium Sized Rechargeable Lithium /Batteries and Battery Systems*, Radio Technical Commission for Aeronautics (RTCA), Dec 2013. Document no. RTCA DO-347.

[7] *Technical Standard Order TSO-C179a, Permanently Installed Rechargeable Lithium Cells, Batteries, and Battery Systems*, Federal Aviation Administration, Apr 2011.

[8] "UN Manual of Tests and Criteria, Seventh Revised Edition," Tech. Rep. ST/SG/AC.10/11/Rev.7, United Nations, 2019.

[9] Lilly, J., "Aviation Propulsive Lithium-Ion Battery Packs State-of-Charge and State-of-Health Estimations and Propulsive Battery System Weight Analysis," *M.S. Aerospace Engineering Thesis*, Embry Riddle Aeronautical University, 2017, p. 96. URL https://commons.erau.edu/cgi/viewcontent.cgi?article=1366&context=edt.

[10] Darcy, E., Darst, J., Walker, W., Finegan, D., and Shearing, P., "Design Guidelines for Safe, High Performing Li-ion Batteries with 18650 cells," *JSC Exploratory Research Workshop*, Petten, Netherlands, 2018. URL https://ec.europa.eu/jrc/sites/jrcsh/files/eric-darcy-nasa-lessons-learned-passive-thermal-runaway-propagation-resistant-designs-spacecraft-batteries.pdf.

[11] Lambe, A. B., and Martins, J. R. R. A., "Extensions to the Design Structure Matrix for the Description of Multidisciplinary Design, Analysis, and Optimization Processes," *Structural and Multidisciplinary Optimization*, Vol. 46, 2012, pp. 273–284. doi:10.1007/s00158-012-0763-y.

[12] Alnæs, M. S., Blechta, J., Hake, J., Johansson, A., Kehlet, B., Logg, A., Richardson, C., Ring, J., Rognes, M. E., and Wells, G. N., "The FEniCS Project Version 1.5," *Archive of Numerical Software*, Vol. 3, No. 100, 2015. doi:10.11588/ans.2015.100.20553.

[13] Julia Billman, W. W., "Battery Failure Databank," *NASA 2020 Battery Workshop*, NASA Tech Report Server, 2020, p. 5. URL https://www.nasa.gov/sites/default/files/atoms/files/nabw20_batt_failure_databank_wwalker.pdf.

[14] Jeon, D. H., and Baek, S. M., "Thermal modeling of cylindrical lithium ion battery during discharge cycle," *Energy Conversion and Management*, Vol. 52, No. 8, 2011, pp. 2973 – 2981. doi:https://doi.org/10.1016/j.enconman.2011.04.013, URL http://www.sciencedirect.com/science/article/pii/S0196890411001439.

[15] Roth, E. P., "Thermal Abuse Performance of MOLI, Panasonic and Sanyo 18650 Li-Ion Cells," *Sandia Report*, Sandia National Laboratories, 2005, p. 54. URL http://prod.sandia.gov/techlib/access-control.cgi/2004/046721.pdf.

[16] Harsh Bhundiya, B. D., Melany Hunt, "Measurement of the Effective Radial Thermal Conductivities of 18650 and 26650 Lithium Ion Battery Cells ," *TFAWS*, NASA Thermal and Fluids Analysis Workshop, 2018, p. 12. URL https://tfaws.nasa.gov/wp-content/uploads/TFAWS18-IN-08_Paper.pdf.

[17] Walker, W., "Short Course on Lithium-ion Batteries: Fundamental Concepts, Battery Safety, and Modeling Techniques," *NASA Battery Workshop*, NASA Technical Report Server, 2019, p. 95. URL https://ntrs.nasa.gov/api/citations/20190030819/downloads/20190030819.pdf.

[18] Daniel Sakoda, L. B. D., Ronald Phelps, "REPORT OF NAPSAT1 BATTERY THERMAL CONTACT RESISTANCE TESTING, MODELING AND SIMULATION," *Space Systems Academic Group*, US Naval Postgraduate School, 2012, p. 37. URL https://apps.dtic.mil/dtic/tr/fulltext/u2/a566672.pdf.

Appendices

A. Additional Figures

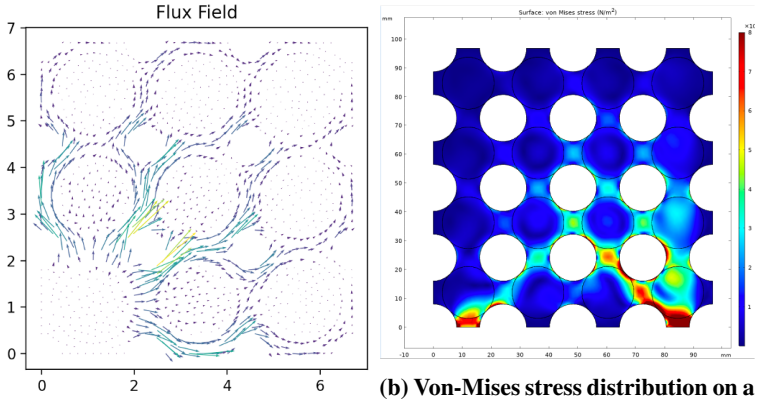

(a) Thermal flux arrow plot

(b) Von-Mises stress distribution on a pack subjected to crash loads

Fig. 11 Supplemental analyses to be explored in future works

B. Aircraft Standards Considered

The following documents were reviewed and found to lack requirements that specifically impact lithium-ion battery pack weight. They are included here as they indirectly impact the aircraft development cycle and aircraft integration.

Table 5 Other Aircraft Standards Documents

Designator	Title
14 CFR Part 23/25/33/35	Code of Federal Regulations Normal Category/Transport Category/Aircraft Engines/ Propellers
AC 20-107B	Composite Aircraft Structure
AIAA G-077	Guide for the Verification and Validation of Computational Fluid Dynamics Simulations
AIAA S-136	Battery Safety Standard for Space Applications
ANSI/AIAA S-144	Large, Prismatic Li-ion Space Cell
GLM-QE-8715.1	Battery Safety and Design Manual for Payloads
IEEE 1625-2008	IEEE Standard for Rechargeable Batteries for Multi-Cell Mobile Computing Devices
IEEE 1725-2011	IEEE Standard for Rechargeable Batteries for Cellular Telephones
ISO TC-197	Basic Considerations for the Safety of Hydrogen Systems
MIL-HDBK-17-1F	Volume 1. Polymer Matrix Composites Guidelines for Characterization of Structural Materials
MIL-PRF-32052	Performance Specification for Batteries, Rechargeable, Sealed
MIL-STD-1541A	[CANCELLED] Electromagnetic Compatibility Requirements for Space Systems (Alternatives listed in $MIL-STD-1541A\_Notice-1$)
MIL-STD-464C	Electromagnetic Environmental Effects, Requirements for Systems
MIL-STD-461F	Requirements for The Control of Electromagnetic Interference Characteristics of Subsystems and Equipment
MIL-STD-704F	Aircraft Electric Power Characteristics
MIL-STD-810	Environmental Engineering Considerations and Laboratory Tests
NASA-RP-1353	Primary Battery Design and Safety Guidelines Handbook
NASA-SSP-41172U	Qualification and Acceptance Environmental Test Requirements
NASA-STD-0005	NASA Configuration Management (cm) Standard
NASA-STD-5001B	Structural Design and Test Factors of Safety for Spaceflight Hardware
NASA-STD-7009	Standard for Models and Simulations
NASA-TM-2005-213995	Preliminary Results of NASA Li-ion Cell Verification Testing for Aerospace Applications
NASA-TM-2008-215154	Progress of Ongoing NASA Li-ion Cell Verification Testing for Aerospace Applications
NAVSEA S9310-AQ-SAF-010	Technical Manual for Batteries, Navy Lithium Safety Program Responsibilities and Procedures
RTCA DO-178C	Software Considerations in Airborne Systems and Equipment Certification
RTCA DO-254	Design Assurance Guidance for Airborne Electronic Hardware
SAE ARP 4754	Aerospace Recommended Practice
SAE ARP 4761	Guidelines and Methods for Conducting the Safety Assessment Process on Civil Airborne Systems and Equipment
SAE AS50881E	Wiring Aerospace Vehicle
SMC-S-008	Electromagnetic Compatibility Requirements for Space Equipment and Systems
SMC-S-017	Li-ion Battery for Spacecraft Applications
TOR-2007-8583-1	Li-ion Battery Standards for Spacecraft Applications
TOR-2007-8583-2	Acquisition Standard for Li-ion Based Launch Vehicle Batteries
TOR-2008-8583-8215	Space and Missile Center Compliance Specifications and Standards